


Nonclassical states of light in a nonlinear Michelson interferometer

Bijoy John Mathew * and Anil Shaji 

Indian Institute of Science Education and Research Thiruvananthapuram, Maruthamala PO, Thiruvananthapuram, Kerala, 695551 India

 (Received 14 June 2021; revised 8 November 2021; accepted 17 November 2021; published 3 December 2021)

Nonlinear quantum metrology schemes can lead to faster than Heisenberg-limited scalings for the measurement uncertainty. We study a Michelson interferometer embedded in a Kerr medium [Phys. Rev. A **92**, 022104 (2015)] that leads to nonlinear, intensity dependent phase shifts corresponding to relative changes in the lengths of its two arms. The quantum Cramér-Rao bound on the minimum achievable measurement uncertainties is worked out and the requirements, in practice, to saturate the bound are investigated. The choice of input state of light into the interferometer and the readout strategy at the output end are discussed. The ideal nonclassical states of light that must be used to saturate the bound are found to be highly susceptible to photon loss noise. We identify optimal states at each noise level that are both resilient to noise and capable of giving the enhanced sensitivities and discuss practical implementations of the interferometry scheme using such states.

DOI: [10.1103/PhysRevA.104.062604](https://doi.org/10.1103/PhysRevA.104.062604)

I. INTRODUCTION

The ability to make precise measurements is a crucial requirement in experimental physics as we continue to explore the boundaries of our knowledge of the physical universe. Detection of gravitational waves via measurement of optical phase generated by a passing wave in an interferometer is one such area where the quantum theory of metrology plays a vital role [1–4]. To measure a physical parameter, a suitable probe whose state evolves in a manner that depends on the value of the parameter is used. The value of the parameter is estimated by a readout of the final state of the probe. If the probe is made of N independent identical classical systems, each of which is capable of giving an estimate of the parameter, then it is well known that the measurement uncertainty in the parameter is shot-noise limited and scales as $1/\sqrt{N}$ [5]. If the measuring device is an interferometer in which the value of the parameter to be measured is imprinted as a phase shift, then N stands for the number of photons in the laser light traversing the interferometer. The $1/\sqrt{N}$ scaling of the measurement uncertainty is also known as the standard quantum limit (SQL).

Quantum metrology refers to the scenario in which the quantum features of the N physical systems that make up the probe can be taken advantage of for achieving better precision in the measurement. Since all physical systems are quantum mechanical in nature to the best of our knowledge, quantum metrology also addresses the question of the fundamental limits on the measurement precision given the constraints on the resources available for performing a measurement. The number N of systems that make up the probe is effectively a placeholder for the specific physical resource like energy, momentum, time, particle number, etc., that is relevant for the measurement being considered. It is known that by utilizing the quantum features of the probe units, one can go beyond the

shot-noise-limited scaling and get to the so-called Heisenberg-limited scaling of $1/N$ for the measurement uncertainty. In the case of interferometry, several schemes have been proposed that theoretically approach the Heisenberg limit by using nonclassical states of light such as maximally entangled NOON states, squeezed states, etc. [6–13]. Some of these quantum metrology protocols have been implemented in gravitational wave interferometers [2–4].

One of the assumptions that goes into obtaining the $1/N$ scaling is that each of the probe units couple independently to the parameter being measured. In other words, the coupling Hamiltonian that generates the parameter-dependent evolution has the form

$$H_{\text{probe}} = \phi \sum_j h_j, \quad j = 1, \dots, N, \quad (1)$$

where ϕ is the measured parameter and h_j are operators on each of the units of the quantum probe. However, if an effective nonlinear coupling can be engineered between the probe units and the parameter, then a faster scaling than $1/N$ for the measurement uncertainty can be achieved. Nonlinear transformations leading to a metrological advantage was considered in the context of interferometry in Ref. [14] and this idea was developed further in Ref. [15]. Using nonlinear generators of parameter-dependent evolution in the context of metrology in general to obtain faster than $1/N$ scaling was first discussed in Ref. [16] and later in Ref. [17]. Possible means of implementing such measurement schemes using atomic systems, Bose-Einstein condensates, etc. were considered in Refs. [18–22] while special cases like restricting the input product states and separable states were considered in Refs. [23–26]. Laboratory implementations of such schemes have also been attempted [27–29]. Whether the enhanced scaling can be thought of as an improvement over Heisenberg-limited scaling or if it is the resource counting that has to change with the introduction of the nonlinear coupling is a matter of debate. For simplicity and clarity, we steer clear

*bijoy13@iisertvm.ac.in

of this question and state directly that we will be referring to the enhanced scaling (anything faster than $1/N$) as super-Heisenberg scaling.

The best possible scaling for the measurement precision for a given probe Hamiltonian can be obtained in terms of the operator seminorm, $\|H_{\text{probe}}\|$, of the coupling Hamiltonian (linear or nonlinear) that generates the parameter-dependent evolution of the probe [16]. For any initial state of the probe and coupling Hamiltonian, H_{probe} , the best possible precision is given by the quantum Cramér-Rao bound [30–33]. Achieving the bound that saturates the best possible scaling possible determined by $\|H_{\text{probe}}\|$ usually involves using highly entangled initial states of the probe. These states typically are not at all robust against external noise and decoherence. However, with nonlinear couplings in H_{probe} , it has been shown that faster than $1/N$ scaling can still be obtained using semiclassical or product states of the probe even if the best possible scaling is not achieved. Such states tend to be more robust against decoherence [15,24,26]. In the context of interferometry, effective nonlinearities that can potentially lead to super-Heisenberg metrology have been demonstrated in light propagation through Kerr-nonlinear media [34–36]. Recently, Luis and Rivas [37] introduced a quantum detection scheme using a Michelson interferometer embedded in gas with Kerr nonlinearity as a candidate system that can demonstrate super-Heisenberg scalings. Coherent light pulses are used as input states in the scheme and light pulse duration was treated as a new variable that comes into play in the measurement.

In this paper, we use the same interferometry scheme as Luis and Rivas but generalize its scope substantially by considering nonclassical states of light as inputs instead of the coherent states considered in Ref. [37]. We recap the nonlinear interferometer in Sec. II, and in Sec. III we compute the quantum Cramér-Rao bound as applicable to this case and find the best theoretically possible scaling for the measurement uncertainty for such an interferometer configuration with and without photon loss noise. We examine the actual performance of the interferometry scheme against the quantum Cramér-Rao bound in Sec. IV. To achieve the theoretical bounds on the measurement uncertainty in practical implementations, both the input state of light into the interferometer as well as the final readout of the output state can both be optimized. We explore both of these optimizations for the cases with and without photon loss. Finally, in Sec. V we identify an optical nonclassical state light that can be used in such an interferometer which leads to the best possible measurement precision while at the same time being resilient to photon loss noise. Our conclusions are in Sec. VI.

II. THE NONLINEAR INTERFEROMETER

Luis and Rivas considered a Michelson interferometer embedded in a gas exhibiting a Kerr nonlinearity. Classical light pulses (coherent states) are injected into one of the input ports of the interferometer while the other input is kept empty with only the quantum vacuum entering that port. A passing gravitational wave signal x manifests itself as anticorrelated length changes of the two arms of the interferometer given by $l_1 = l_0 - x/2$, $l_2 = l_0 + x/2$, where l_0 is the original length of each arm. The changes in length are computed from the

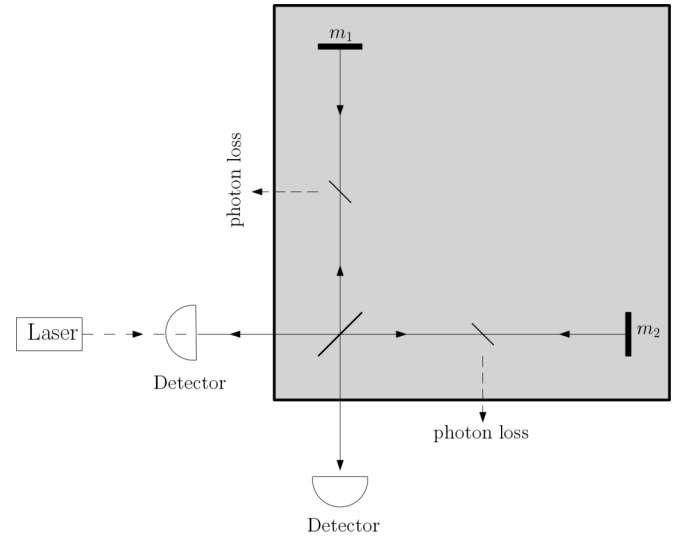


FIG. 1. Schematic diagram for a Michelson interferometer embedded in a Kerr medium [37]. Photon loss can be modeled as beam splitters in each arm that remove a fraction of the photons in that arm.

changes in the relative phase of the light in the two arms that, in turn, is detected by counting the number of photons coming out at each output port of the interferometer [1]. A schematic diagram of the interferometer is given in Fig. 1. The refractive index of the Kerr medium that envelopes the interferometer has an intensity-dependent term leading to the nonlinearity in the relevant Hamiltonian operator that generates the relative phase between the two arms. The refractive index of the gas can be expressed as

$$n = n_0 + \tilde{n}I = n_0(1 + \chi N), \quad (2)$$

where n_0 is the linear index, N is the number of photons circulating in the interferometer, \tilde{n} is a coefficient related to the third-order susceptibility $\chi^{(3)}$ of the Kerr medium that quantifies the nonlinearity of the refractive index, and χ , which is proportional to $\chi^{(3)}$, captures the nonlinear phase shift per photon.

Photons that enter the interferometer arms from the beam splitter pick up the phase shift while propagating through the arms, bounce back from the mirrors, rejoin at the beam splitter and are finally detected at the output ports. Light propagation is described in terms of the internal modes of the interferometer, a_1, a_2 , by the unitary operator $U = U_1 U_2$, where

$$U_j = e^{i\phi_j \hat{G}_j}, \quad \hat{G}_j = \hat{N}_j + \frac{\chi}{2} \hat{N}_j^2. \quad (3)$$

In the equation above, $\phi_j = \bar{k}l_j$, $j = 1, 2$ where \bar{k} is the wave number of the light used and $\hat{N}_j = a_j^\dagger a_j$ is the photon number operator for each arm. The two detectors at the output ports of interferometer record the difference in the number of photons detected at each port, allowing us to infer the relative phase difference between the arms of the interferometer. In the following, instead of applying the beam-splitter transformation on the state of light that has traversed through the interferometer so as to find the state at the output ports of the interferometer, we take the measurement operator corresponding to the difference in photocounts at the output ports,

$M' = (b_2^\dagger b_2 - b_1^\dagger b_1)$, with b_1, b_2 being the external modes of the interferometer, and apply on it the (inverse) beam-splitter transformation to find its form immediately before the returning light hits the beam splitter. This choice makes most of our calculations significantly simpler. The corresponding measurement operator in terms of the internal modes is

$$M = i(a_2^\dagger a_1 - a_1^\dagger a_2). \quad (4)$$

When a coherent state is injected into one of the input ports of the interferometer as in Ref. [37], the measurement uncertainty, as quantified by the standard deviation of the estimate of x obtained from the measurement of M , is found to scale as $1/N^{3/2}$.

The choice of the input state considered by Luis and Rivas is typical of interferometers, including those typically used for gravitational wave detection. The readout of the state of light at the output end also conforms to such a typical configuration. However, these choices do not necessarily represent ones that correspond to the absolute minimum possible measurement uncertainty that can be achieved using such an interferometer configuration with a nonlinear phase shift. We explore the minimum possible uncertainty in the next couple of sections.

III. THEORETICAL BOUND ON THE MEASUREMENT UNCERTAINTY

The super-Heisenberg scaling of $1/N^{3/2}$ is not the best possible scaling for the interferometry scheme considered here. The theoretical bound on the measurement uncertainty is given by the quantum Cramér-Rao bound (QCRB) that in turn is phrased in terms of the quantum Fisher information [30–33]. The quantum state of light in the interferometer is effectively the quantum probe in this case. The QCRB captures the idea that the measurement uncertainty is inversely proportional to the rate of change of the state of the probe in its Hilbert space in response to changes in the measured parameter (phase ϕ in the present case). As mentioned earlier, the bound on the measurement uncertainty given by the QCRB depends only on the input state of light and the parameter-dependent dynamics that it goes through within the interferometer. The bound is independent of the particular readout strategy that is employed to determine the relevant information from the final state of the probe that then leads to the estimate of the parameter of interest. Once the QCRB is known, one still has to find the best readout strategy on the output probe state that either saturates the bound or comes close to it given the practical limitations of a laboratory interferometer setup. Before considering these questions, we first compute the QCRB with and without photon loss noise for the nonlinear interferometry scheme.

A. Ideal case: No photon loss

We write the part of the probe Hamiltonian that imprints the relative phase ϕ on the light in the interferometer as $H_\phi = \phi H$. The change in the state of light, ρ , with respect to changes in ϕ is generated by the operator H as

$$\rho' = \frac{\partial \rho}{\partial \phi} = -i[H, \rho]. \quad (5)$$

The quantum Cramér-Rao bound for the measurement uncertainty in estimating ϕ is then given in terms of the quantum Fisher information \mathcal{F} as [33]

$$(\delta\phi)^2 \geq \frac{1}{\nu\mathcal{F}} = \frac{1}{\nu\langle\mathcal{L}_\rho^2(\rho')\rangle}, \quad (6)$$

where ν is the number of times the measurement is repeated and \mathcal{L} is the symmetric logarithmic derivative operator. The measurement uncertainty decrease obtained via the repetition factor ν is not important to our framework, so we ignore it for the rest of the analysis. Now, $\mathcal{L}_\rho(\rho')$ can be expressed in the basis $\{|j\rangle\}$ that diagonalizes ρ as [32]

$$\mathcal{L}_\rho(\rho') = \sum_{p_j+p_k \neq 0} \frac{2}{p_j+p_k} \rho'_{jk} |j\rangle\langle k|, \quad (7)$$

where $\rho'_{jk} = \langle j|\rho'|k\rangle$ and $\{p_j\}$ are the eigenvalues of ρ . The quantum Fisher information can then be written using Eq. (5) as

$$\mathcal{F} = 4 \left[\sum_j p_j (\langle j|H^2|j\rangle - |\langle j|H|j\rangle|^2) - \sum_{j \neq k} \frac{4p_j^2 p_k}{(p_j + p_k)^2} |\langle j|H|k\rangle|^2 \right]. \quad (8)$$

From Eq. (3), assuming $\phi_2 = \phi/2$ and $\phi_1 = -\phi/2$, the generator of the relative phase ϕ for the interferometry scheme can be written as

$$H = \frac{\hat{G}_2 - \hat{G}_1}{2}. \quad (9)$$

A quantum state of light that is constructed by superposing eigenstates of H that correspond to its largest and smallest eigenvalues is a good candidate for the optimal probe state that changes rapidly with small changes in ϕ . Adding to this the requirement that the initial state of the probe that we consider also be one with a fixed photon number would lead us to the “NOON” state,

$$|\psi\rangle_{\text{NOON}} = \frac{|N, 0\rangle + |0, N\rangle}{\sqrt{2}}.$$

However, for reasons that will become clear in Sec. IV, we consider a more general state of the form

$$|\psi\rangle = \frac{|N-k, k\rangle + |k, N-k\rangle}{\sqrt{2}}, \quad k \in [0, N]. \quad (10)$$

Note that $|\psi\rangle$ is the state entering the interferometer arms after the beam splitter and is not the state that is injected into the input port(s). To obtain the state that has to be injected, the inverse-beam-splitter transformation may be applied. Note that for NOON states, $k=0$. The state of light reaching the beam splitter after propagation through the interferometer arms is

$$U|\psi\rangle = \frac{1}{\sqrt{2}} [e^{i\phi_1 \tilde{G}_{N-k}} e^{i\phi_2 \tilde{G}_k} |N-k, k\rangle + e^{i\phi_1 \tilde{G}_k} e^{i\phi_2 \tilde{G}_{N-k}} |k, N-k\rangle], \quad (11)$$

where $\tilde{G}_n = n + \frac{\chi}{2}n^2$. Here we have assumed that the changes produced in the optical phase by sources other than the gravitational wave signal x are negligible.

Since the state of light in the interferometer in the ideal case without noise is always a pure state, Eq. (8) reduces to

$$\begin{aligned} \mathcal{F} &= 4(\Delta H)^2 = (\tilde{G}_{N-k} - \tilde{G}_k)^2 \\ &= \left(N - 2k + \frac{\chi N^2}{2} - \chi Nk \right)^2. \end{aligned} \quad (12)$$

The Fisher information is maximum when $k = 0$ so that all the terms with negative signs in the expression for \mathcal{F} above are zero. This choice corresponds to the initial state being the NOON state. In this case $\sqrt{\mathcal{F}} \sim N^2(\chi/2 + 1/N)$. Since the relative phase ϕ is directly proportional to x , ($\phi = \bar{k}x$), the QCRB on the measurement uncertainty in estimating the change in length of the arms of the interferometer is

$$\delta x \sim \delta\phi \geq \frac{1}{\sqrt{\mathcal{F}}} \sim \frac{1}{\chi N^2}. \quad (13)$$

As shown in Ref. [16], $1/N^2$ scaling is the best that can be expected with the $\chi N^2/2$ (quadratic) nonlinearity considered here. The QCRB tells us that using the optimal standard deviation Δx for any configuration of the interferometer can scale at best as $1/N^2$, which beats the usual Heisenberg limit by a factor of $1/N$.

B. With photon loss

All practical interferometers are invariably affected by decoherence and the dominant source of noise is usually photon loss. This photon loss can be modeled by inserting beam splitters on both arms of the interferometer with transmissivities, η_{a_1} and η_{a_2} , respectively, as shown in the schematic in Fig. 1. They can be inserted both before or after the phase is picked up by photons in the interferometer, as these operations commute with each other. The completely positive, trace-preserving map that describes this model of photon loss is [38]

$$\rho_n = \sum_{p,q=0}^{\infty} K_{a_1,q} K_{a_2,p} \rho_0 K_{a_2,p}^\dagger K_{a_1,q}^\dagger, \quad (14)$$

where

$$\begin{aligned} K_{a_1,q} &= (1 - \eta_{a_1})^{q/2} \eta_{a_1}^{a_1^{\dagger} a_1/2} \frac{a_1^q}{\sqrt{q!}}, \\ K_{a_2,p} &= (1 - \eta_{a_2})^{p/2} \eta_{a_2}^{a_2^{\dagger} a_2/2} \frac{a_2^p}{\sqrt{p!}}. \end{aligned} \quad (15)$$

Setting $\eta_{a_1} = \eta_{a_2} = \eta$ and applying this map on the state in Eq. (11), we get

$$\begin{aligned} \rho_n &= \sum_{q,p=0} \left[\frac{B_{pq}}{2} \sqrt{P_{ppqq}^k} |n_q^{N-k}, n_p^k\rangle\langle n_q^{N-k}, n_p^k| \right] \\ &+ \sum_{q,p=0} \left[e^{-i\phi G(k)} \frac{B_{pq}}{2} \sqrt{P_{ppqq}^k} |n_q^{N-k}, n_p^k\rangle\langle n_q^k, n_p^{N-k}| \right] \end{aligned}$$

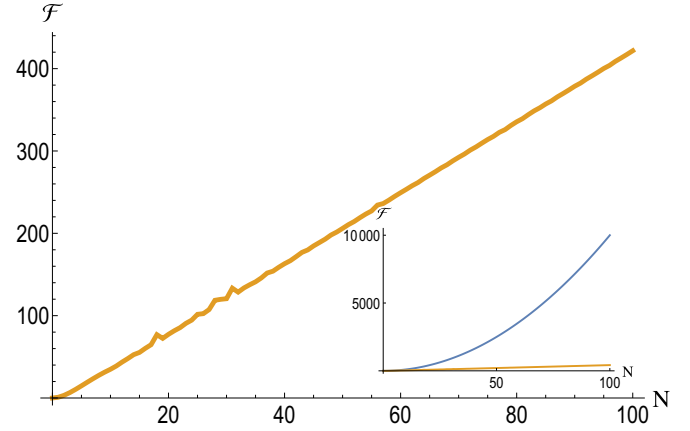


FIG. 2. Maximum quantum Fisher information as a function of N for the state in Eq. (16) with the transmission coefficient of the beam splitter modeling the photon loss set at $\eta = 0.9$. We see that the Fisher information scales linearly with N and the super-Heisenberg scaling is lost when there is photon loss. In the inset, a comparison of the quantum Fisher information with and without photon loss, setting $\eta = 1$ and $\eta = 0.9$, respectively, is shown. Note that \mathcal{F} , as given in Eq. (8), is plotted on the y axis both in the main graph as well as in the inset. The (blue) curve in the inset corresponding to $\eta = 1$ appears quadratic even if the behavior is actually quartic in N since the coefficient of the N^4 term in Eq. (12) is proportional to $\chi \ll N$. The quartic behavior will be evident only for much larger values of N than what we have considered here.

$$\begin{aligned} &+ \sum_{q,p=0} \left[e^{i\phi G(k)} \frac{B_{pq}}{2} \sqrt{P_{qqpp}^k} |n_q^k, n_p^{N-k}\rangle\langle n_q^{N-k}, n_p^k| \right] \\ &+ \sum_{q,p=0} \left[\frac{B_{pq}}{2} \sqrt{P_{qqpp}^k} |n_q^k, n_p^{N-k}\rangle\langle n_q^k, n_p^{N-k}| \right], \end{aligned} \quad (16)$$

where $B_{pq} = (1 - \eta)^{p+q} \eta^{N-p-q} / p!q!$ with $G(k) = \tilde{G}_{N-k} - \tilde{G}_k$, and $P_{abcd}^k = P(k, a)P(k, b)P(N-k, c)P(N-k, d)$, with $P(i, j) = i!/(i-j)!$. In Eq. (16), the photon number in each of the Fock states is represented as $n_s^r = r - s$. The upper limits of the summations in the equation are the photon numbers of the states appearing in each term in the absence of photon loss (k and $N - k$).

The quantum Fisher information corresponding to the state with photon losses included was obtained numerically. We set the value of χ as 10^{-8} considering the giant nonlinearities reported in Ref. [39]. The quantum Fisher information is computed for up to $N = 100$ and for all cases corresponding to $k \in [0, N]$ and the maximum overall k is taken. For low values of the photon loss, the maximum occurs when k takes values at the ends of the interval $[0, N]$ corresponding to the NOON state. For larger losses, the maximum of the quantum Fisher information occurs for values of k that are slightly away from the ends of the interval. The plot of maximum of the quantum Fisher information versus N is shown in Fig. 2 for beam splitter transmissivities $\eta = 0.9$ and $\eta = 1$ (zero photon loss), respectively. It can be seen that with merely 10% photon loss, the quadratic relationship between the maximum of the quantum Fisher information and the number of photons that

goes beyond the Heisenberg limit in the absence of noise is quickly reduced to a linear one.

IV. READOUT OF THE PROBE

The QCRB predicts that the best-case scenario for the nonlinear interferometer is an input state of the type in Eq. (10). As mentioned earlier, the bound is independent of the readout procedure used to gather the information about ϕ and x from the final state of the probe. In the interferometer we consider, the readout is photon counting at the output ports that corresponds to measurement of the operator M given in Eq. (4). The signal x , through the phase difference $\Delta\phi = \phi_2 - \phi_1$ it creates between the interferometer arms as it passes by, would produce a shift in the mean value of M . We had concluded by looking at Eq. (12) that $k = 0$ maximizes the quantum Fisher information. However, it is easy to see from Eqs. (4) and (11) that the state of light at the output ports, in the case without noise, leads to a nonzero value for $\langle M \rangle$ only if $k = (N + 1)/2$ or $k = (N - 1)/2$. This highlights a problem that is often glossed over in quantum metrology. The nature of the quantum probe can lead to practical limitations on the types of readouts that can be done on it. This means that, in some cases, physical and practical considerations may limit one's ability to saturate the QCRB and it becomes meaningful to consider only the lowest achievable measurement uncertainty in the presence of the limitations on readout [40].

In our case, for practical implementation, we therefore restrict to $k = (N + 1)/2$ or $k = (N - 1)/2$, and we consider the input state (assuming N to be odd)

$$|\psi\rangle = \frac{1}{\sqrt{2}} \left[\left| \frac{N-1}{2}, \frac{N+1}{2} \right\rangle + \left| \frac{N+1}{2}, \frac{N-1}{2} \right\rangle \right]. \quad (17)$$

After going through the interferometer arms, the state becomes

$$|\psi\rangle = \frac{1}{\sqrt{2}} \left[e^{i\frac{\phi}{2}(G_{N+1} - G_{N-1})} \left| \frac{N-1}{2}, \frac{N+1}{2} \right\rangle + e^{-i\frac{\phi}{2}(G_{N+1} - G_{N-1})} \left| \frac{N+1}{2}, \frac{N-1}{2} \right\rangle \right]. \quad (18)$$

For this state we get,

$$\begin{aligned} \langle M \rangle &= \left(\frac{N+1}{2} \right) \sin \left[\phi (\tilde{G}_{\frac{N+1}{2}} - \tilde{G}_{\frac{N-1}{2}}) \right] \\ &= \left(\frac{N+1}{2} \right) \sin \left[\bar{k}x \left(1 + \frac{\chi}{2}N \right) \right], \end{aligned} \quad (19)$$

where \bar{k} is the wave number of the (monochromatic) light used. For the state in Eq. (18), the variance $\langle \Delta M^2 \rangle = \langle M^2 \rangle - \langle M \rangle^2$ is

$$\langle \Delta M^2 \rangle = \left(\frac{N+1}{2} \right)^2 \left\{ \cos^2 \left[\bar{k}x \left(1 + \frac{\chi}{2}N \right) \right] + 1 \right\} - 2. \quad (20)$$

The standard deviation in the estimate of x is obtained using straightforward error propagation as

$$\bar{k}\Delta x = \Delta\phi = \frac{\sqrt{\langle \Delta M^2 \rangle}}{|d\langle M \rangle/dx|}, \quad (21)$$

leading to

$$\Delta x \simeq \frac{2\sqrt{2}}{\chi N}, \quad (22)$$

for large N and $x \rightarrow 0$ indicating that, despite the nonlinearity in the interferometer, the restriction on the read-out procedure constrains the scaling of the measurement uncertainty to the Heisenberg-limited one. However, this does not mean that the nonlinearity is not useful. If the nonlinear medium were absent, the minimum measurement uncertainty scales in this case as $1/\sqrt{N}$ when using the N photons as independent probes of x . An improvement by a factor $1/\chi\sqrt{N}$ is therefore provided by the nonlinearity in this case.

Multiphoton coincidence as readout

It is known that multiphoton coincidence detection has to be implemented at the output end if the full advantage provided by NOON states in the noiseless case is to be obtained [41–43]. These readouts, however, are typically extremely challenging to implement. A few recent attempts towards implementing multiphoton coincidence detection can be found in Refs. [44,45]. We consider m -photon coincidence measurements at the output end described by the operator,

$$M_m = i[(a_1^\dagger)^m (a_2)^m - (a_1)^m (a_2^\dagger)^m], \quad (23)$$

where we have written M_m as it appears before the final beam splitter transformation for simplicity.

When the state of light just before the last beam splitter of the interferometer is given by Eq. (11), we obtain

$$\langle M_m \rangle = C_{N,m} \sin \left[\left(m + \frac{\chi}{2}Nm \right) \phi \right],$$

where we have chosen $k = (N - m)/2$ and

$$C_{N,m} = \frac{\left(\frac{N+m}{2} \right)!}{\left(\frac{N-m}{2} \right)!}.$$

Using $\langle M_m^2 \rangle = C_{N,m}^2$ we find

$$\langle \Delta M_m^2 \rangle = C_{N,m}^2 \cos^2 \left[\left(m + \frac{\chi}{2}Nm \right) \phi \right],$$

and

$$\Delta x \simeq \Delta\phi = \frac{\sqrt{\langle \Delta M_m^2 \rangle}}{|\partial \langle M_m \rangle / \partial \phi|} = \frac{2}{\chi Nm + m}. \quad (24)$$

When $m = N$ and $k = 0$, we saturate the quantum Cramér-Rao bound given in Eq. (13) with $\Delta x \sim 2/\chi N^2$ to leading order in $1/N$. If we add photon losses, then the multiphoton coincidence measurements also fail to give super-Heisenberg scaling, and the measurement uncertainty follows the same behavior as in Fig. 2 for the QCRB. It may be noted that alternate strategies like Bayesian estimation protocols [46] can be used to saturate the quantum Cramér-Rao bound using measurement operators like M rather than M_m . However, this is a multiround protocol in which the measurement sensitivity improves progressively and each instance using N photons is not always equivalent to the previous one. This makes it more difficult to understand clearly the effect of photon loss on the measurement sensitivity while using such protocols. To keep

the discussion as clear as possible, we consider only the multiphoton coincidence measurements in the ensuing discussion on finding an optimal initial state that gives the $1/N^2$ scaling even in the presence of photon loss.

V. OPTIMAL INITIAL STATE

The extreme susceptibility of the enhanced scaling of the measurement uncertainty when using NOON-type states leads us to the question of whether an optimal input state that is robust to noise can be found. As input into the interferometer, we start from a general superposition state of the form

$$|\psi\rangle = \sum_{k=0}^{\tau} \alpha_k \{|N-k, k\rangle + |k, N-k\rangle\}, \quad (25)$$

where τ is $(N-1)/2$ if N is odd, $N/2$ if N is even and the coefficients, α_i , are chosen such that the state as a whole is normalized. Note that we have chosen to keep the total photon number fixed for the state at N . This places the resource counting at an equal footing between the optimal state and the NOON-type states we previously considered. We are not considering the more general case of a superposition that keeps the mean photon number fixed.

Under the action of the unitary that corresponds to propagation along the interferometer arms along with the photon loss as described by Eq. (14) (considering equal loss in both arms, $\eta_{a_1} = \eta_{a_2} = \eta$), the density matrix of the state of light at the output port takes the following form:

$$\begin{aligned} \rho_n = & \sum_{q,p,k,l} [B_{pq}^{kl} e^{i\frac{\phi}{2}[G(k)-G(l)]} \sqrt{P_{ppqq}^{kl}} |n_q^{N-k}, n_p^k\rangle \langle n_q^{N-l}, n_p^l|] \\ & + \sum_{q,p,k,l} [B_{pq}^{kl} e^{i\frac{\phi}{2}[G(k)+G(l)]} \sqrt{P_{ppqq}^{kl}} |n_q^{N-k}, n_p^k\rangle \langle n_q^l, n_p^{N-l}|] \\ & + \sum_{q,p,k,l} [B_{pq}^{kl} e^{-i\frac{\phi}{2}[G(k)+G(l)]} \sqrt{P_{qqpp}^{kl}} |n_q^k, n_p^{N-k}\rangle \langle n_q^{N-l}, n_p^l|] \\ & + \sum_{q,p,k,l} [B_{pq}^{kl} e^{-i\frac{\phi}{2}[G(k)-G(l)]} \sqrt{P_{qqpp}^{kl}} |n_q^k, n_p^{N-k}\rangle \langle n_q^l, n_p^{N-l}|], \end{aligned} \quad (26)$$

where $B_{pq}^{kl} = (\alpha_k \alpha_l^*) B_{pq}$ and

$$P_{abcd}^{kl} = P(k, a)P(l, b)P(N-k, c)P(N-l, d).$$

The sums over q and p run from 0 to $k, l, N-k$ or $N-l$ as the case may be for the states on the right of the sum while k and l run from 0 to τ .

The quantum Fisher information can be computed numerically for the state in Eq. (26) corresponding to different values of the photon loss. The coefficients, α_k , are then optimized while keeping the state normalized so as to give maximum Fisher information. This optimization was done for up to $N = 25$ and the results are plotted in Fig. 3. It is clear from Fig. 3 that the super-Heisenberg scaling for the measurement uncertainty is not fully destroyed in the case of the optimal input state even in the presence of photon loss noise, unlike in the case of the NOON-type states. Even with 60% photon loss, the super-Heisenberg scaling is observed to persist. In the inset plot from Fig. 3, we also compare

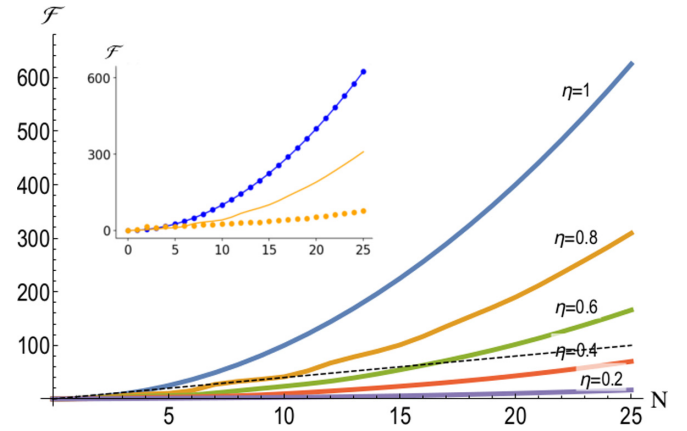


FIG. 3. Maximum of the quantum Fisher information for the state in Eq. (26) vs N varying values of photon losses. Note that η is the transmission coefficient of the beam splitters that model the photon loss and so smaller values of η correspond to greater photon losses. The Heisenberg-limited scaling is the dashed black line for comparison. In the inset, a comparison of performances of the HB state (dotted) and our optimal initial state (solid line) is plotted for $\eta = 1$ (blue) and $\eta = 0.8$ (orange).

our results with the well-known Holland-Burnett (HB) states, which have been shown to attain the Heisenberg limit for phase estimation while maintaining some robustness towards decoherence [47,48]. We see that, while the HB states match the performance of the optimal states that we consider in the zero-loss case, this is not the case when photon losses are present. The scheme with an optimized superposition of fixed photon number states as input is seen to provide advantageous scaling for the measurement uncertainty as well as much-improved robustness against photon loss.

The fixed photon number states in Eq. (25) are characterized by the amplitudes α_k that are optimized so as to give the largest possible quantum Fisher information for each value of η . In Fig. 4, the distribution of $|\alpha_k|^2$ of the optimal states are shown for different values of η with $N = 25$. We see that, as expected, when there is no photon loss only α_0 is nonzero and the optimal state is the NOON state. When photon losses are present, other values of α_k become nonzero. For $N = 25$, there are 13 different amplitudes defining the state. However, note that even for rather large photon losses, the distribution is limited to small values of k with $|\alpha_k|^2$ for $k > 5$ becoming negligible relative to the other amplitudes.

Readout of the optimal state

The readout procedure that would, in practice, saturate the QCRB for the optimal state and lead to super-Heisenberg scalings for the measurement uncertainty even in the presence of noise is theoretically a measurement along the basis given by the eigenstates of the symmetric logarithmic derivative operator in Eq. (7). Implementing such measurements is not feasible in practice. The two-photon coincidence measurement of the standard interferometric set up again is not suitable for the optimal N -photon state we consider. We therefore explore the effectiveness of the m -photon coincidence measurement from Eq. (23) with $m = N$.

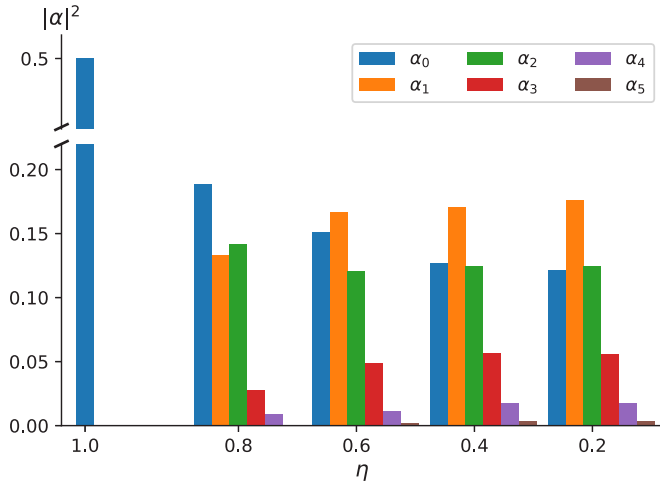


FIG. 4. The distributions of the absolute values squares of the first six coefficients, α_k , of the optimal state in Eq. (25) are shown for different values of η for $N = 25$. With no losses, only $\alpha_0 \neq 0$ and as the losses increase the peak of the distribution shifts to higher values of k . Note that the y axis of the figure is broken so as to show all the distributions clearly in the same scale.

The measurement uncertainty is numerically calculated via error propagation with the measurement operator M_N acting on the state in Eq. (26) and α_i optimized for maximizing the Fisher information given the photon loss. In the absence of photon loss, when the NOON state is used, $\langle M_N \rangle$ oscillates sinusoidally. In principle, the measurement uncertainty Δx for any value of ϕ has to be the same according to Eq. (24). However, as can be seen from the same equation, those values of ϕ for which $\partial \langle M_N \rangle / \partial \phi$ vanishes are not particularly good operating points in real experiments as well as for numerical computation. So we have to minimize the numerically evaluated measurement uncertainty for all values of $\phi \in [0, \pi]$, which makes the computation challenging.

The inverse of the measurement uncertainty in Fig. 5 is plotted as a function of N for easy comparison with the QFI.

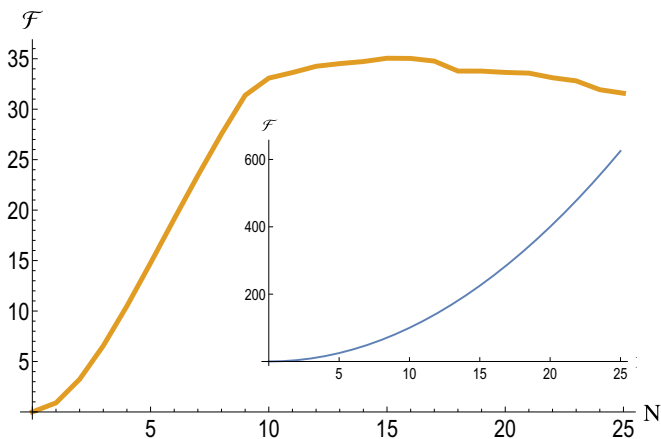


FIG. 5. Inverse of the measurement uncertainty ($1/\Delta x$) vs N for the optimized state in Eq. (26) with the photon loss coefficient set to $\eta = 0.9$. Super-Heisenberg scaling is obtained for small values of N but the curve soon saturates. The inset is the $\eta = 1$ case.

We see that measuring M_N can achieve the best scaling offered by the optimized initial state in the absence of any photon loss. Using M_N for the readout is the best choice when NOON states are used as input into the interferometer. The same measurement is not the ideal one for the optimal states that are resilient to photon loss. With only 10% loss, the nonlinear scaling is very quickly lost and the plot eventually saturates. For very small N , the optimal states are relatively close in form to the NOON state and readout using M_N still gives a measurement uncertainty that saturates the QCRB. However, when N increases, this is no longer the case. This behavior is not completely unexpected because the presence of noise can fundamentally limit the ability to saturate the ultimate super-Heisenberg limit for asymptotically large values of N irrespective of input states or readout methods [49]. An alternate measurement strategy can be evolved that maintains nonlinear scaling for higher N . This involves a further optimization over the measurement operator also which we have not attempted due to the numerical complexity involved. In addition, just like the best possible measurement given by the eigenstates of the symmetric logarithmic derivative operator, the optimized measurement need not be amenable to experimental implementation, either.

VI. CONCLUSION

We have shown that the nonlinear interferometric setup of Luis and Rivas [37] can give super-Heisenberg scaling for the measurement uncertainty when using nonclassical states of the NOON type. The quantum Cramér-Rao bound for the interferometric setup was computed when NOON-type, fixed photon-number states were used, and we found that the measurement uncertainty can, in principle, scale as $1/N^2$, beating the Heisenberg-limited scaling of $1/N$. However, we also found that, if the readout strategy employed on the quantum state of light at the output ports of the interferometer is limited to two-photon coincidences, then the QCRB is not achievable. This brought into focus a potential issue that is often glossed over in the theoretical literature on quantum-limited metrology, namely, the achievability, in practice of the QCRB. We do find, however, that even with such limitations on the readout strategy, the nonlinear scheme performs better than the linear one.

We also addressed the problem of extreme susceptibility of the NOON-type states to photon loss noise. In the presence of even very small amounts of photon loss, we see that the QCRB deteriorates rapidly to scalings that are equal to or even slower than Heisenberg-limited scaling. The quantum advantage, as well as the additional advantage provided by the nonlinear coupling, are both found to be extremely fragile with photon loss. Keeping the overall photon number of the input state fixed, we found an optimal state that provides both super-Heisenberg scaling as well as robustness against photon-loss noise by numerically optimizing a generic input state with fixed total photon number. We examined the performance of this state in a practically implementable scheme with N -photon coincidences and found that super-Heisenberg scaling can be obtained for low N . Finding the optimal readout strategy that can saturate the QCRB for all N while

maintaining the robustness of the scheme against decoherence due to photon loss are avenues to be explored in the future.

Since embedding the interferometer in a nonlinear Kerr medium is impractical for LIGO-type interferometers, it would be more interesting to consider the case where a small section of the interferometer is embedded in such a nonlinear medium. It has been observed that Kerr media and radiation pressure both introduce intensity-dependent nonlinearities [50] in the state of light. By carefully choosing a medium with the appropriate sign and magnitude for its nonlinearity, radiation pressure noise can be compensated for, improving the sensitivity of the interferometer [51]. Combined usage of nonclassical input states along with smaller

Kerr cells inside the interferometer arms could, in principle, lead to a viable and practical implementation of a robust, high-precision interferometer.

ACKNOWLEDGMENTS

A. Shaji acknowledges the support of SERB, Department of Science and Technology, Government of India through Grant No. EMR/2016/007221 and the QuEST program of the Department of Science and Technology through Project No. Q113 under Theme 4. Both authors acknowledge the center for high performance computing of IISER TVM for the use of the *Padmanabha* cluster.

-
- [1] R. X. Adhikari, *Rev. Mod. Phys.* **86**, 121 (2014).
 [2] The LIGO Scientific Collaboration, *Nat. Phys.* **7**, 962 (2011).
 [3] H. Grote, K. Danzmann, K. L. Dooley, R. Schnabel, J. Slutsky, and H. Vahlbruch, *Phys. Rev. Lett.* **110**, 181101 (2013).
 [4] J. Aasi *et al.*, *Nat. Photonics* **7**, 613 (2013).
 [5] V. Giovannetti, S. Lloyd, and L. Maccone, *Nat. Photonics* **5**, 222 (2011).
 [6] C. M. Caves, *Phys. Rev. D* **23**, 1693 (1981).
 [7] B. Yurke, S. L. McCall, and J. R. Klauder, *Phys. Rev. A* **33**, 4033 (1986).
 [8] J. J. Bollinger, W. M. Itano, D. J. Wineland, and D. J. Heinzen, *Phys. Rev. A* **54**, R4649 (1996).
 [9] H. Lee, P. Kok, and J. P. Dowling, *J. Mod. Opt.* **49**, 2325 (2002).
 [10] V. Giovannetti, S. Lloyd, and L. Maccone, *Phys. Rev. Lett.* **96**, 010401 (2006).
 [11] B. L. Higgins, D. W. Berry, S. D. Bartlett, H. M. Wiseman, and G. J. Pryde, *Nature (London)* **450**, 393 (2007).
 [12] D. W. Berry, B. L. Higgins, S. D. Bartlett, M. W. Mitchell, G. J. Pryde, and H. M. Wiseman, *Phys. Rev. A* **80**, 052114 (2009).
 [13] L. Pezzè, A. Smerzi, M. K. Oberthaler, R. Schmied, and P. Treutlein, *Rev. Mod. Phys.* **90**, 035005 (2018).
 [14] A. Luis, *Phys. Lett. A* **329**, 8 (2004).
 [15] J. Beltrán and A. Luis, *Phys. Rev. A* **72**, 045801 (2005).
 [16] S. Boixo, S. T. Flammia, C. M. Caves, and JM Geremia, *Phys. Rev. Lett.* **98**, 090401 (2007).
 [17] A. Luis, *Phys. Rev. A* **76**, 035801 (2007).
 [18] A. M. Rey, L. Jiang, and M. D. Lukin, *Phys. Rev. A* **76**, 053617 (2007).
 [19] S. Choi and B. Sundaram, *Phys. Rev. A* **77**, 053613 (2008).
 [20] S. Boixo, A. Datta, M. J. Davis, A. Shaji, A. B. Tacla, and C. M. Caves, *Phys. Rev. A* **80**, 032103 (2009).
 [21] M. Napolitano and M. W. Mitchell, *New J. Phys.* **12**, 093016 (2010).
 [22] A. B. Tacla, S. Boixo, A. Datta, A. Shaji, and C. M. Caves, *Phys. Rev. A* **82**, 053636 (2010).
 [23] S. M. Roy and S. L. Braunstein, *Phys. Rev. Lett.* **100**, 220501 (2008).
 [24] S. Boixo, A. Datta, S. T. Flammia, A. Shaji, E. Bagan, and C. M. Caves, *Phys. Rev. A* **77**, 012317 (2008).
 [25] S. Boixo, A. Datta, M. J. Davis, S. T. Flammia, A. Shaji, and C. M. Caves, *Phys. Rev. Lett.* **101**, 040403 (2008).
 [26] A. Rivas and A. Luis, *Phys. Rev. Lett.* **105**, 010403 (2010).
 [27] M. Napolitano, M. Koschorreck, B. Dubost, N. Behbood, R. J. Sewell, and M. W. Mitchell, *Nature (London)* **471**, 486 (2011).
 [28] R. J. Sewell, M. Napolitano, N. Behbood, G. Colangelo, F. Martin Ciurana, and M. W. Mitchell, *Phys. Rev. X* **4**, 021045 (2014).
 [29] G. Tóth and I. Apellaniz, *J. Phys. A: Math. Theor.* **47**, 424006 (2014).
 [30] C. Helstrom, *Phys. Lett. A* **25**, 101 (1967).
 [31] C. W. Helstrom, *J. Stat. Phys.* **1**, 231 (1969).
 [32] S. L. Braunstein and C. M. Caves, *Phys. Rev. Lett.* **72**, 3439 (1994).
 [33] S. L. Braunstein, C. M. Caves, and G. Milburn, *Ann. Phys. (NY)* **247**, 135 (1996).
 [34] A. F. Pace, M. J. Collett, and D. F. Walls, *Phys. Rev. A* **47**, 3173 (1993).
 [35] H. Rehbein, J. Harms, R. Schnabel, and K. Danzmann, *Phys. Rev. Lett.* **95**, 193001 (2005).
 [36] A. Khalaidovski, A. Thüring, H. Rehbein, N. Lastzka, B. Willke, K. Danzmann, and R. Schnabel, *Phys. Rev. A* **80**, 053801 (2009).
 [37] A. Luis and A. Rivas, *Phys. Rev. A* **92**, 022104 (2015).
 [38] R. Demkowicz-Dobrzanski, U. Dorner, B. J. Smith, J. S. Lundeen, W. Wasilewski, K. Banaszek, and I. A. Walmsley, *Phys. Rev. A* **80**, 013825 (2009).
 [39] L. Spani Molella, R.-H. Rinkleff, G. Kühn, and K. Danzmann, *Appl. Phys. B: Lasers Opt.* **90**, 273 (2008).
 [40] S. Jose, N. Jaseem, and A. Shaji, *Phys. Rev. A* **87**, 022330 (2013).
 [41] J. A. Jones, S. D. Karlen, J. Fitzsimons, A. Ardavan, S. C. Benjamin, G. A. D. Briggs, and J. J. L. Morton, *Science* **324**, 1166 (2009).
 [42] I. Afek, O. Ambar, and Y. Silberberg, *Science* **328**, 879 (2010).
 [43] Y. Israel, S. Rosen, and Y. Silberberg, *Phys. Rev. Lett.* **112**, 103604 (2014).
 [44] D. Branning, S. Khanal, Y. H. Shin, B. Clary, and M. Beck, *Rev. Sci. Instrum.* **82**, 016102 (2011).
 [45] D. Zhu, Q.-Y. Zhao, H. Choi, T.-J. Lu, A. E. Dane, D. Englund, and K. K. Berggren, *Nat. Nanotechnol.* **13**, 596 (2018).
 [46] L. Pezzè and A. Smerzi, *Phys. Rev. Lett.* **100**, 073601 (2008).
 [47] M. J. Holland and K. Burnett, *Phys. Rev. Lett.* **71**, 1355 (1993).
 [48] A. Datta, L. Zhang, N. Thomas-Peter, U. Dorner, B. J. Smith, and I. A. Walmsley, *Phys. Rev. A* **83**, 063836 (2011).
 [49] B. M. Escher, R. L. de Matos Filho, and L. Davidovich, *Nat. Phys.* **7**, 406 (2011).
 [50] R. Loudon, *Phys. Rev. Lett.* **47**, 815 (1981).
 [51] R. S. Bondurant, *Phys. Rev. A* **34**, 3927 (1986).